Stability and non-equilibrium physics in holography

Yu Tian

University of Chinese Academy of Sciences

Numerical Relativity and Holography
June 27, 2016
Santiago de Compostela, Spain

- W.-J. Li, YT and H. Zhang, JHEP 1307 (2013) 030 [arXiv:1305.1600].
- Y. Du, C. Niu, YT and H. Zhang, JHEP 1512 (2015) 018 [arXiv:1412.8417].
- Y. Du, S.-Q. Lan, YT and H. Zhang, JHEP 1601 (2016) 016 [arXiv:1511.07179].
- M. Guo, C. Niu, YT and H. Zhang, PoS Modave2015 (2016) 003 [arXiv:1601.00257].
- M. Guo, C. Niu, S. Lan, YT and H. Zhang, CQG 33 (2016) 127001 [arXiv:1602.03824].
- R. Li, YT, H. Zhang and J. Zhao, [arXiv:1604.01535].
- H. Zeng, YT, Z. Fan and C.-M. Chen, Phys. Rev. D 93 (2016) 121901(R) [arXiv:1604.08422].
- S.-Q. Lan, YT and H. Zhang, *Towards Quantum Turbulence in Finite Temperature Bose-Einstein Condensates*, [arXiv:1605.01193].
- ...

Holography from string theory: AdS/CFT

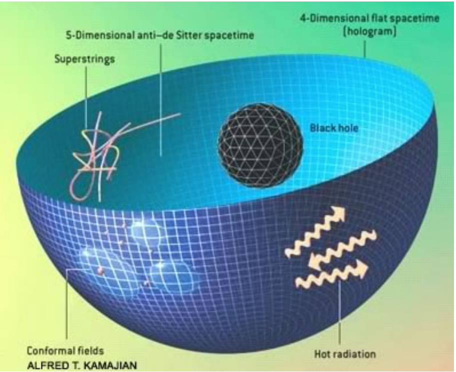

$$Z_{CFT}[J] = Z_{AdS}[\bar{\phi}(= J)] \Longrightarrow Z^c_{CFT}[J] \approx I^{os}_{AdS}[\bar{\phi}]$$

Facts about (applied) AdS/CFT

- Finite temperature field theory with finite chemical potential is dual to a charged black hole in the bulk AdS:

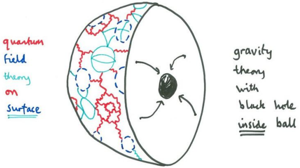

Temperature	$\longleftrightarrow$	Hawking temperature
Chemical potential	$\longleftrightarrow$	Potential

- Motivation of applied AdS/CFT: understanding difficult physics (on the boundary) by AdS (classical) gravity
- Two ways of applied AdS/CFT: top-down and bottom-up

Why is applied AdS/CFT needed?

- Controllable manipulations of various quantum many-body systems (BEC, QGP, ...)

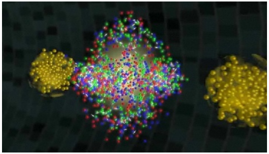

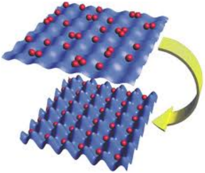

- Lack of (even phenomenological) theories for the dissipative, far-from-equilibrium and strongly coupled systems
  Example: Gross-Pitaevskii equation (for BEC)

$$(i-\eta)\hbar\partial_t\varphi = (-\frac{\nabla^2}{2m} + V(t,\mathbf{x}) + g|\varphi|^2 - \mu)\varphi$$

Applied AdS/CFT: subjects

- AdS/QCD
  Hadron spectrum, thermalization of QGP, hydrodynamics of QGP, ...
- AdS/CMT (condensed matter theory)
  Superfluids and superconductors, charge density waves, entanglement entropy, many-body localization, ...
- AdS/???

Applied AdS/CFT: trends

- Towards less symmetric configurations:

$$\text{Isotropic} \longrightarrow \text{Anisotropic}$$
$$\text{Homogeneous} \longrightarrow \text{Inhomogeneous}$$

- Towards fully numerical relativity regimes:

$$\text{Without backreaction} \longrightarrow \text{With backreaction}$$

Figure: Computational Holography!

- Action of the simplest holographic model

  [Hartnoll, Herzog and Horowitz, arXiv:0803.3295]

$$I = \int_{\mathcal{M}} d^4x\sqrt{-g}\frac{1}{q^2}(-\frac{1}{4}F_{AB}F^{AB} - |D\Psi|^2 - m^2|\Psi|^2).$$

- Background metric

$$ds^2 = \frac{L^2}{z^2}[-f(z)dt^2 - 2dtdz + dx^2 + dy^2], \quad f(z) = 1 - \frac{z^3}{z_h^3}.$$

- Heat bath temperature

$$T = \frac{3}{4\pi z_h}.$$

- Equations of motion

$$D_A D^A\Psi - m^2\Psi = 0, \quad \nabla_A F^{AB} = i(\Psi^* D^B\Psi - C.C.).$$

- The radial gauge $A_z = 0$
- Asymptotic behavior at the AdS boundary

$$A_\nu = a_\nu + b_\nu z + o(z),$$
$$\Psi = L^{-1}[\psi_- z + \psi_+ z^2 + o(z^2)], \quad m^2 = -2L^{-2}.$$

- AdS/CFT dictionary

$$\langle J^\nu \rangle = \frac{\delta I_{ren}}{\delta a_\nu} = \lim_{z\to 0} \frac{\sqrt{-g}}{q^2} F^{z\nu},$$
$$\langle O \rangle = \frac{\delta I_{ren}}{\delta \psi_-} = \frac{1}{q^2}(\psi_+^* - \dot{\psi}_-^* - i a_t \psi_-^*),$$

where

$$I_{ren} = I - \frac{1}{Lq^2} \int_{\mathcal{B}} \sqrt{-\gamma} |\Psi|^2$$

is the renormalized bulk action.

- Charge density $(q=1)$

$$\rho \equiv \langle J^t \rangle = -\lim_{z\to 0} \partial_z A_t = -b_t.$$

- Chemical potential (in equilibrium)

$$\mu = \lim_{z\to 0} A_t = a_t$$

with $A_t(z_h) = 0$ required by regularity at the horizon.

- Pseudo-spectral methods to solve differential equations
Expanding unknown functions by polynomials or Fourier modes, or (almost) equivalently, sampling the unknown functions by collocation points, which turns the differential equations into (systems of) algebraic equations.

Thermodynamic stability and phase transition

- Grand canonical ensemble (with μ fixed)
  Minimize the grand potential

$$\Omega = T \ln Z(\mu) = T I^{os}_{AdS}(a_t)$$

- Canonical ensemble (with ρ fixed)
  Minimize the Helmholtz free energy

$$F = T \ln Z(\rho) = T I^{os}_{AdS}(-b_t)$$

- Turn off the source ($\psi_- = 0$) and compare the trivial solution and the hairy ones ($\psi_+ \neq 0$, $\langle O \rangle = \psi_+^*$)
- The metal-superconductor phase transition in the HHH model

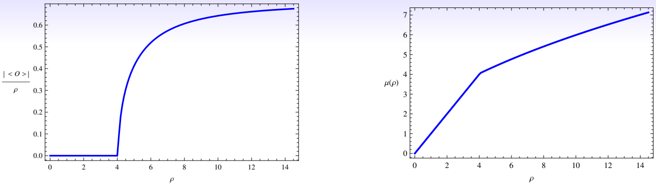

Figure: The condensate $\langle O \rangle$ and chemical potential μ as a function of charge density with the critical charge density $\rho_c = 4.06$ ($\mu_c = 4.06$).

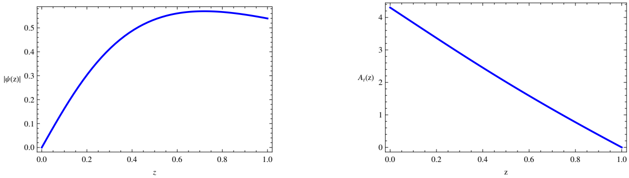

Figure: The profile of amplitude of scalar field and electromagnetic potential for the superconducting phase at the charge density $\rho = 4.7$.

Multiple orders: the BHMRS model

[Basu, He, Mukherjee, Rozali and Shieh, arXiv:1007.3480]

The action is

$$I = \int dx^4 \sqrt{-g}\left(-\frac{1}{4}F^{AB}F_{AB} - |D_1\psi_1|^2 - |D_2\psi_2|^2 - m_2^2|\psi_2|^2\right)$$

with

$$D_1 = \nabla - iq_1 A, \quad D_2 = \nabla - iq_2 A,$$

under the same bulk metric as in the HHH model. Particularly, choose

$$m_2^2 = -2L^{-2}, \quad q_1 = 1.95, \quad q_2 = 1.$$

The two orders corresponding to the two scalars tend to compete.

The condensates and phase structure

- Generically, the two orders expel each other, which makes the window of coexistence very narrow.

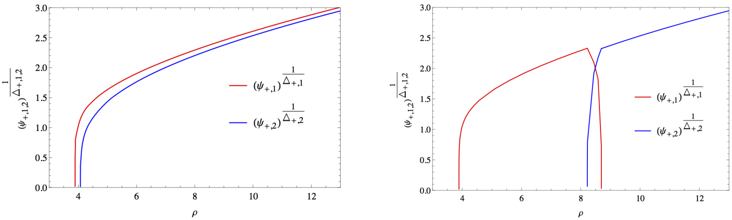

Figure: The condensates with respect to the charge density ρ in the BHMRS model.

- In the back-reacted case, whenever the coexisting phase appears, it is thermodynamically more favorable under the grand canonical ensemble [Cai *et al*, arXiv:1307.2768].

Time evolution and dynamic (in)stability of the BHMRS model

- Coordinate choices for time-dependent problems in holography: Schwarzschild vs Eddington

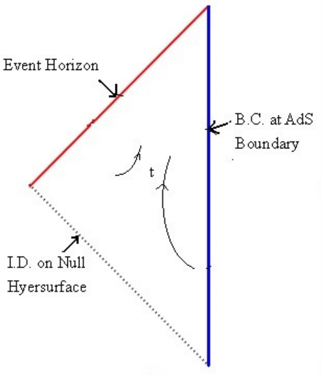

Figure: Work in the infalling Eddington coordinates

[Y.-Q. Du, YT, H. Zhang and S. Lan, arXiv:1511.07179]

- Dynamic (in)stability under linear perturbations, described by the quasi-normal modes (QNM) $\delta\Phi \sim e^{-i\omega t}$
- In the fully coupled case and under the infalling Eddington coordinates, our efficient strategy for QNM ($\psi \equiv \psi_2/z$):

$$\delta\psi_1 = p(z)e^{-i\omega t} + \bar{p}(z)e^{i\omega^* t},$$
$$\delta\psi = q(z)e^{-i\omega t} + \bar{q}(z)e^{i\omega^* t},$$
$$\delta A_t = \frac{1}{i}[a(z)e^{-i\omega t} - a^*(z)e^{i\omega^* t}].$$

The gauge redundancy can be removed by the boundary condition $a|_{z=0} = 0$.

Focusing on the $e^{-i\omega t}$ terms, there are simple rules for obtaining the "static" linear perturbation equation from the linearized equations of motion for $(\delta\psi_1, \delta\psi, \delta A_t)$:

$$\begin{aligned} \delta\psi_1 &\to p, \qquad & \delta\psi_1^* &\to \bar{p}^* \\ \delta\psi &\to q, \qquad & \delta\psi^* &\to \bar{q}^* \\ \delta A_t &\to -ia_t, \qquad & \partial_t &\to -i\omega \end{aligned}$$

Importantly, it can be generally shown that $(p^*, \bar{p}, q^*, \bar{q}, a_t^*)$ decouples from $(p, \bar{p}^*, q, \bar{q}^*, a_t)$, with the final equations for both sets of variables being complex conjugate to each other.

Anyway, substitution of the above expressions into the equations of motion (and the appropriate boundary conditions) yields the "static" linear perturbation equation

$$L(\omega)\begin{pmatrix} p \\ \bar{p}^* \\ q \\ \bar{q}^* \\ a \end{pmatrix} = 0,$$

which under numerical methods is just a system of homogeneous linear algebraic equations. That the above system has nontrivial solutions means

$$\det[L(\omega)] = 0,$$

which is the nonlinear equation that determines ω (QNM).

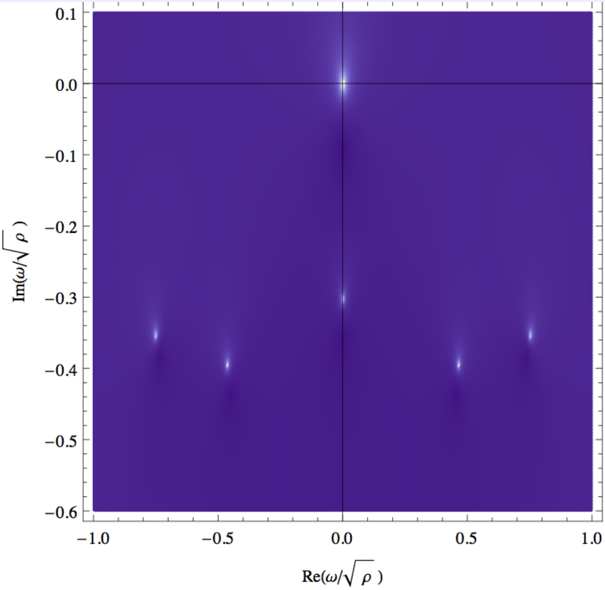
0.1
0.0
−0.1
−0.2
−0.3
−0.4
−0.5
−0.6
Im(ω/√ρ)
−1.0
−0.5
0.0
0.5
1.0
Re(ω/√ρ)

Comments on different strategies for QNM (in holography):

- Schwarzschild vs Eddington
  [Leaver, 1990; ...]
- gauge invariant vs gauge dependent
  [Amado, Kaminski and Landsteiner, 2009; Bhaseen, Gauntlett, Simons, Sonner and Wiseman, 2012; ...]
- separation of real and imaginary parts $\psi = a + ib$
  versus
  introduction of complex conjugate $\psi \to (\psi, \psi^*)$

- Dynamic evolution of holographic systems (real time holography for non-equilibrium physics)
  The HHH model as an example ($\psi \equiv \Psi/z$, $L = 1 = z_h$):

$$\partial_t \partial_z A_t = -i(\psi^* \partial_t \psi - \psi \partial_t \psi^*) - 2A_t \psi^* \psi + if(\psi^* \partial_z \psi - \psi \partial_z \psi^*) \quad (1)$$

$$\partial_z^2 A_t = i(\psi^* \partial_z \psi - \psi \partial_z \psi^*) \quad (2)$$

$$2(\partial_t - iA_t)\partial_z \psi - i\partial_z A_t \psi - f\partial_z^2 \psi - f' \partial_z \psi + z\psi = 0 \quad (3)$$

- Constraint equations in the bulk from the U(1) gauge symmetries of the holographic models
  In the above case: three equations for two functions (A_t, ψ)

$$(1) + (3) \Longrightarrow \partial_t (2)$$
$$(2) + (3) \Longrightarrow \partial_z (1)$$

- Choices of the constraint equation: (2) vs (1)
  - (2): $\partial_z^2 A_t = i(\psi^* \partial_z \psi - \psi \partial_z \psi^*)$ holds on the initial surface $t = 0$. Evolve the system using (1) and (3) to the final surface $t = t_f$.

    Pros: The violation of (2) at $t = t_f$ can be checked as an indication of numerical errors (and even coding mistakes).

    Cons: The time accumulated error of (2) is inevitable. Totally untrusted for long time evolution.
  - (1): $\partial_t \rho = 0$ holds on the boundary surface $z = 0$. Prepare the initial value of ψ and then use (3) to evolve the system while using (2) to obtain A_t on every time slice with the boundary conditions $\partial_z A_t|_{z=0} = -\rho$ and $A_t|_{z=0} = \mu$ (gauge fixing).

    Reminder: holographic dictionary

    $$\rho \equiv \langle J^t \rangle = -\lim_{z \to 0} \partial_z A_t$$

    Accumulated error along the z direction. Relatively better for long time evolution.

- The extensively adopted numerical scheme of dynamic evolution:
  - Spectral expansion in the spatial directions (e.g. Chebyshev expansion in the z direction)
  - The 4th order Runge-Kutta method for the time evolution
- For the HHH model, we have used the nonlinear dynamic evolution to study
  - Periodic driving and dynamic phase transition of the holographic superconductor
    [W.-J. Li, YT and H. Zhang, arXiv:1305.1600]
  - Nonlinear charge transport in the holographic superconductor
    [H. Zeng, YT, Z. Fan and C.-M. Chen, arXiv:1604.08422]
- Consistency of the thermodynamic stability and nonlinear dynamic stability in the BHMRS model

Inhomogeneous configurations of the holographic superfluids

- Dark soliton (1d for the boundary system)

  [Keranen, Keski-Vakkuri, Nowling and Yogendran, 2009; ...]

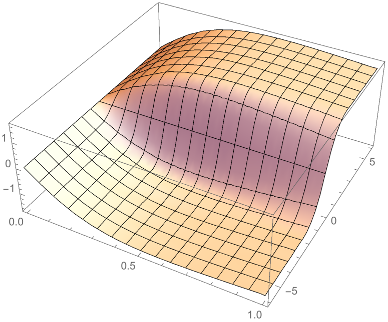

Figure: Bulk profile ($\psi \equiv \Psi/z$) of the holographic dark soliton at the chemical potential $\mu = 6$

- Vortex (2d for the boundary system)

  [Keranen, Keski-Vakkuri, Nowling and Yogendran, 2009; ...]

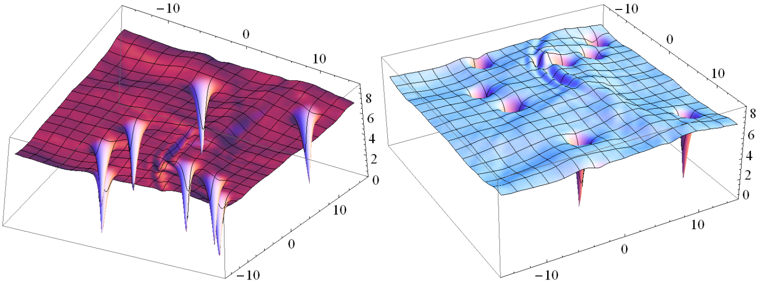

Figure: The bottom and top view of $|\langle O\rangle|$ for the holographic superfluid with vortices at $\mu = 6.25$. The vortex cores are located at the position where the condensate vanishes. [Y. Du, C. Niu, YT and H. Zhang, arXiv:1412.8417]

Dynamics of inhomogeneous holographic superfluids

[Chesler, Liu and Adams, 2012; Ewerz, Gasenzer, Karl and Samberg, 2014; Du, Niu, YT and Zhang, 2014]

- Equations of motion in the inhomogeneous case:

$$\begin{aligned} & \partial_t(\partial_z A_t + \partial\cdot\mathbf{A}) - (\partial^2 A_t + f\partial_z\partial\cdot\mathbf{A}) \\ = \; & -i(\psi^*\partial_t\psi - \psi\partial_t\psi^*) - 2A_t\psi^*\psi + if(\psi^*\partial_z\psi - \psi\partial_z\psi^*) \end{aligned} \tag{4}$$

$$\begin{aligned} & \partial_z(\partial A_t + f\partial_z\mathbf{A}) - 2\partial_t\partial_z\mathbf{A} + \partial^2\mathbf{A} - \partial(\partial\cdot\mathbf{A}) \\ = \; & i(\psi^*\partial\psi - \psi\partial\psi^*) + 2\mathbf{A}\psi^*\psi \end{aligned} \tag{5}$$

$$\partial_z(\partial_z A_t - \partial\cdot\mathbf{A}) = i(\psi^*\partial_z\psi - \psi\partial_z\psi^*) \tag{6}$$

$$2(\partial_t - iA_t)\partial_z\psi - i\partial_z A_t\psi - f\partial_z^2\psi - f'\partial_z\psi - (\partial - i\mathbf{A})^2\psi + z\psi = 0 \tag{7}$$

Here $\mathbf{A} \equiv (A_x, A_y)$, $\partial \equiv (\partial_x, \partial_y)$.

- Five equations for four unknown functions $(A_t, \mathbf{A}, \psi)$

$$(4) + (5) + (7) \Longrightarrow \partial_t(6)$$
$$(5) + (6) + (7) \Longrightarrow \partial_z(4)$$

- Choice of the constraint equation: (6)

$$\partial_z(\partial_z A_t - \partial \cdot \mathbf{A}) = i(\psi^* \partial_z \psi - \psi \partial_z \psi^*)$$

holds on the initial surface $t = 0$. Evolve the system using (4), (5) and (7) to the final surface $t = t_f$.

[A. Adams, P. Chesler and H. Liu, arXiv:1212.0281]

- Choice of the constraint equation: (4)

$$(4)|_{z=0} \Longrightarrow$$

$$\partial_t \rho + \partial \cdot \mathbf{J} = 0 \tag{8}$$

holds on the boundary surface $z = 0$. Prepare the initial value of $(\mathbf{A}, \psi, \rho)$ and then use (5), (7) and (8) to evolve the system while using (6) to obtain A_t on every time slice with the boundary conditions $\partial_z A_t|_{z=0} = -\rho$ and $A_t|_{z=0} = \mu$ (gauge fixing).

Reminder: holographic dictionary

$$\langle J^\nu \rangle = \lim_{z\to 0} \sqrt{-g} F^{z\nu}$$

[Y. Du, C. Niu, YT and H. Zhang, arXiv:1412.8417]

Kolmogorov scaling law and energy cascade in superfluid turbulence

- Superfluid velocity for the order parameter $\varphi(\boldsymbol{x})$:

$$\boldsymbol{u} = \frac{\boldsymbol{j}}{|\varphi|^2}, \qquad \boldsymbol{j} = \frac{i}{2}[\varphi^*(\partial - i\boldsymbol{a})\varphi - \varphi(\partial + i\boldsymbol{a})\varphi^*]$$

- Quantization of circulation of the velocity field:

$$\oint_C d\boldsymbol{x} \cdot \boldsymbol{u} = 2\pi w$$

with the winding number w an integer.

- Kinetic energy density and its spectra:

$$\varepsilon_{kin}(t, \boldsymbol{x}) = \frac{|\varphi|^2}{2}\boldsymbol{u}^* \cdot \boldsymbol{u}$$

$$E_{kin}(t) = \int \varepsilon_{kin}(t, \boldsymbol{x}) d^2\boldsymbol{x} = \int_0^\infty \epsilon_{kin}(t, k) dk,$$

[A. Adams, P. Chesler and H. Liu, arXiv:1212.0281]

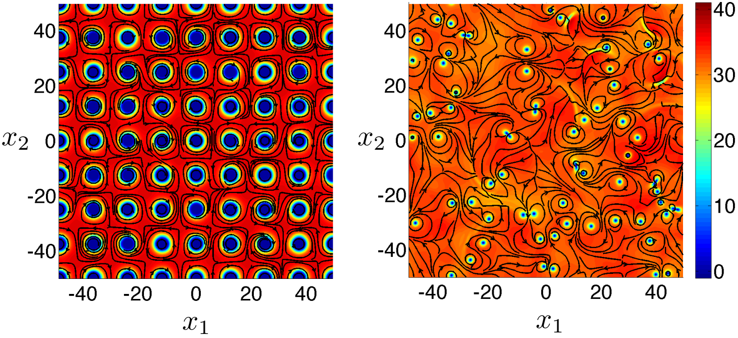

Figure: The superfluid condensate $|\langle O \rangle|^2$ at time $t = 0$ (left) and $t = 300$ (right). The superfluid current circulates around the core of each vortex, where the condensate vanishes. The winding number ± 6 vortices (left) rapidly decay into the winding number ± 1 vortices (right), and then vortices of opposite winding number collide and annihilate.

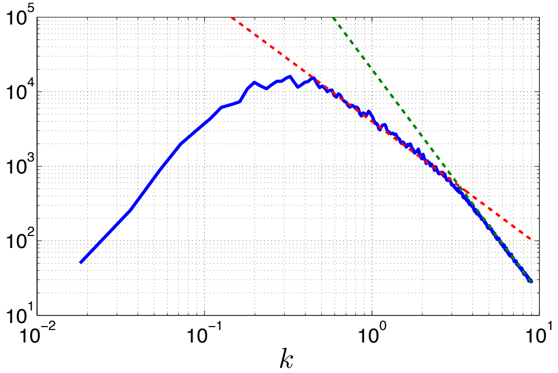

Figure: The energy spectrum $\epsilon_{kin}(t,k)$ at time $t=300$ (quantum turbulence). The red dashed line is the Kolmogorov scaling $k^{-5/3}$ valid in an assumed inertial range, which also appears in the classical turbulence, suggestive of a universal property of turbulence.

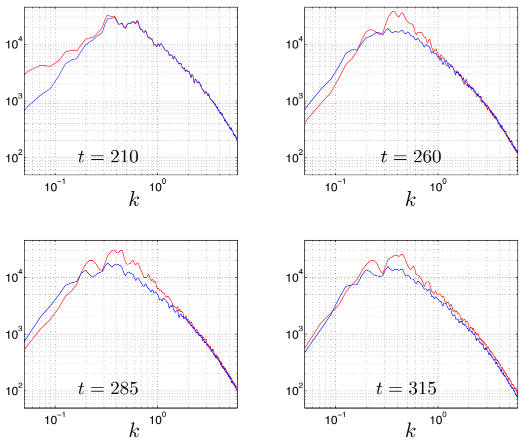

Figure: Energy injection and energy cascade. The blue curve is the energy spectrum with no driving while red curve is that with driving in the IR. Drive adds energy in the IR between times $210 < t < 260$. As time progresses the added energy propagates from the IR to the UV (direct energy cascade) where it is dissipated.

Comments on the energy cascade in classical and quantum turbulence in two spatial dimensions:

- There are indications that the classical turbulence has an inverse energy cascade (from the UV to the IR).
- Phenomenological methods give conflicting conclusions regarding the direction of cascade in superfluid turbulence.

Towards the BEC-BCS crossover in holographic superfluids

- BEC-type and BCS-type superfluidity viewed from the dark solitons in cold atom systems (at zero temperature)

  BEC-type: condensation of interacting bosonic degrees of freedom (molecules of bound fermions)
  density depletion $> 80\%$, tending to 1 in the BEC limit

  Crossover: smooth transition between the BEC side and the BCS side
  density depletion $\approx 80\%$

  BCS-type: condensation of Cooper pairs formed by interacting fermions
  density depletion $< 80\%$, tending to 0 in the BCS limit

[Pitaevskii *et al*, arXiv:0706.0601]

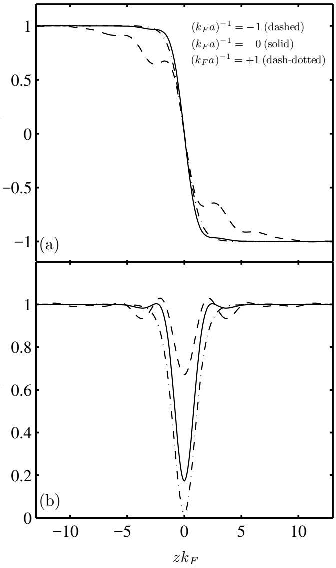

Figure: (a) Order parameter Δ and (b) density n for a dark soliton on the BCS side (dashed line), at the crossover (solid) and on the BEC side (dot-dashed), respectively. Both Δ and n are normalized to their asymptotic values far away from the soliton. [Pitaevskii *et al*, 2007]

- The density depletion is defined as

$$1 - \frac{n}{n_0}$$

at the center of the soliton, where the order parameter vanishes.

- Quantizations in holography: standard vs alternative

$$\Psi = z\psi_- + z^2\psi_+ + o(z^2)$$
$$J_- = \psi_- = 0 \quad \longrightarrow \quad \langle O_+ \rangle = \psi_+^*$$
$$J_+ = \psi_+ = 0 \quad \longrightarrow \quad \langle O_- \rangle = \psi_-^*$$

(static case)

- Density depletion of holographic solitons [Keranen *et al*, 2009]

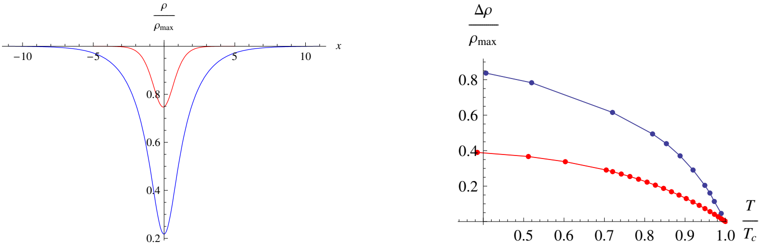

Figure: Left: density depletion for $\mu/\mu_c = 1.9$: $\langle O_- \rangle$ is blue (BEC-like). Right: density depletion as a function of the temperature: $\langle O_- \rangle$ on the top and $\langle O_+ \rangle$ on the bottom.

Universality of the Kolmogorov scaling law and direct energy cascade in (holographic) superfluid turbulence

- Realization of the alternative quantization in the dynamic case

  [Guo, Lan, Niu, YT and Zhang; Lan, YT and Zhang, 2016]

  Under the Eddington coordinates

$$\langle O_+\rangle = \frac{\delta I_+}{\delta\psi_-} = \psi_+^* - \dot{\psi}_-^* - ia_t\psi_-^*, \qquad I_+ \equiv I_{ren}$$

$$\tilde{\psi}_+ \equiv \langle O_+\rangle^* \Longrightarrow \langle O_-\rangle = \frac{\delta I_-}{\delta\tilde{\psi}_+} = -\psi_-^*$$

$$I_- = I + (\int_{\mathcal{B}}\sqrt{-\gamma}n_a\Psi^* D^a\Psi + C.C.) + \int_{\mathcal{B}}\sqrt{-\gamma}|\Psi|^2$$

I_+ and I_- are related by a Legendre transformation.
So the proper boundary condition for a holographic superfluid under the alternative quantization is at $z = 0$

$$\tilde{\psi}_+ = \psi_+ - \dot{\psi}_- + ia_t\psi_- = 0$$

The gauge field sector is the same in both quantizations.

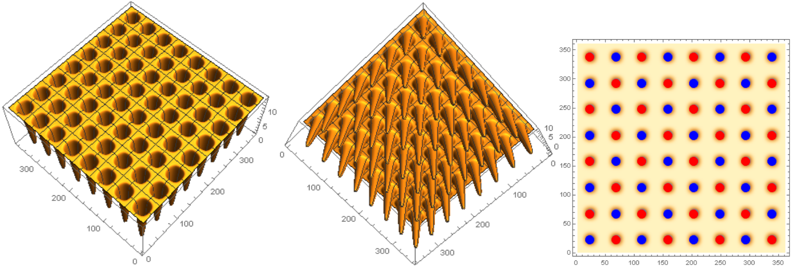

Figure: The initial configuration of the BEC-like superfluid at the chemical potential $\mu = 2 > \mu_c \approx 1.12$. (Anti-)vortices are placed in the periodic box. The first two panels are 3D plots of $|\langle O_- \rangle|^2$. The rightmost panel is the density plot of $|\langle O_- \rangle|^2$ with the red points denoting vortices ($w = 6$) and the blue points denoting anti-vortices ($w = -6$).

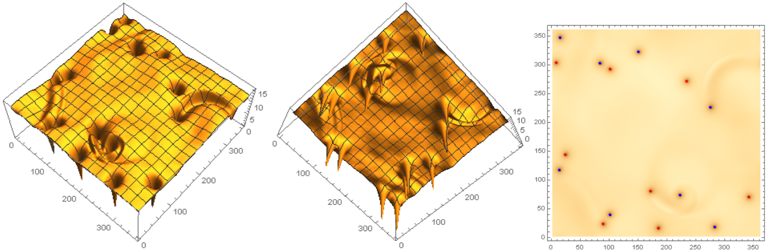

Figure: The later time ($t = 400$) configuration of the turbulent BEC-like superfluid. The first two panels are 3D plots of $|\langle O_- \rangle|^2$. The rightmost panel is the density plot of $|\langle O_- \rangle|^2$ with the red points denoting vortices ($w = 1$) and the blue points denoting anti-vortices ($w = -1$). [S. Lan, YT and H. Zhang, arXiv:1605.01193]

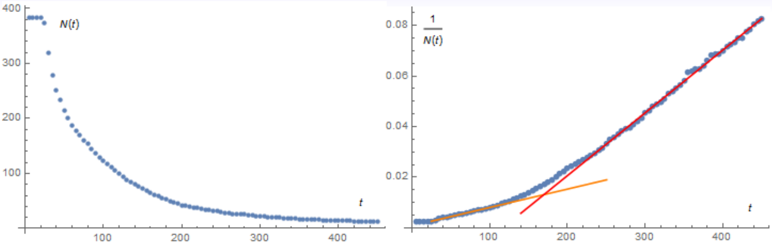

Figure: The temporal evolution of averaged vortex number $N(t)$ (left) and its inverse (right) in the turbulent superfluid over 18 groups of data at the chemical potential $\mu = 2$. The latter was fitted by the behavior $\frac{d}{dt}\frac{1}{N(t)} = \Gamma(t)$, with two constant Γ regions found. Among them the late time $(t > 240)$ linear region is believed to be universal, since it is also observed under the standard quantization in different initial conditions [Ewerz, Gasenzer, Karl and Samberg; Du, Niu, YT and Zhang, 2014] and in cold atom experiments [Kwon *et al*, 2014].

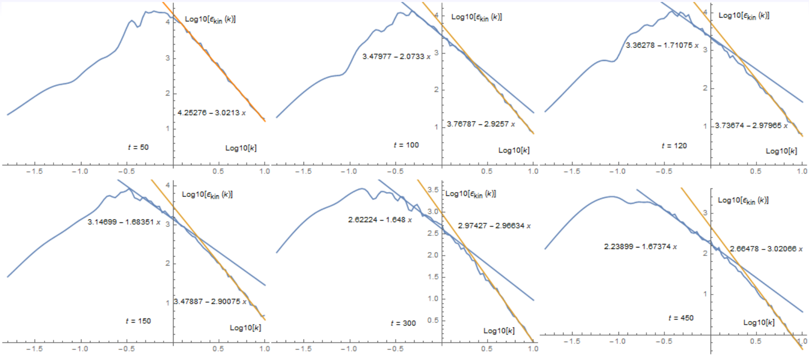

Figure: The kinetic energy spectra $\epsilon_{kin}(t,k)$ at various times for an arbitrarily chosen evolution process at $\mu = 2$. The blue lines are fitting results of the spectra, which are close to the Kolmogorov scaling $k^{-5/3}$. It is noteworthy that the inertial range keeps creeping into the IR as time progresses.

Time	Inertial range in k & x space		Averaged vortex spacing
150	0.33∼1.74,	3.6∼19.0	11.8
200	0.28∼1.74,	3.6∼22.4	15.35
300	0.20∼1.66,	3.8∼31.4	21.32
450	0.16∼1.45,	4.3∼39.3	28.86

Table: The inertial range and averaged vortex spacing at different times, where the averaged vortex spacing is estimated by the formula $\frac{100}{\sqrt{N(t)}}$.

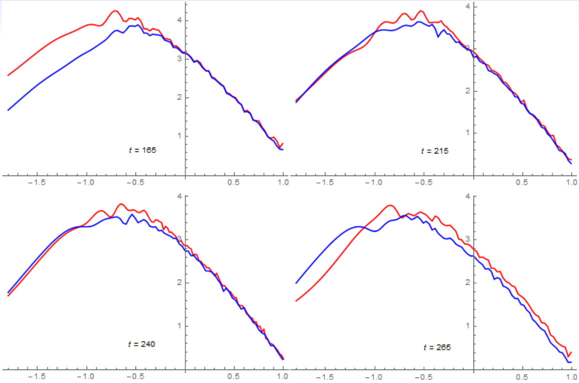

Figure: The comparison of the kinetic energy spectra $\epsilon_{kin}(t,k)$ at various times between the driven and undriven systems. The external sources are turned on at $t = 150$ and turned off at $t = 210$. The blue curve is the kinetic energy spectrum for the undriven BEC-like superfluid while the red one is that for the driven BEC-like superfluid. The direct energy cascade is also observed.

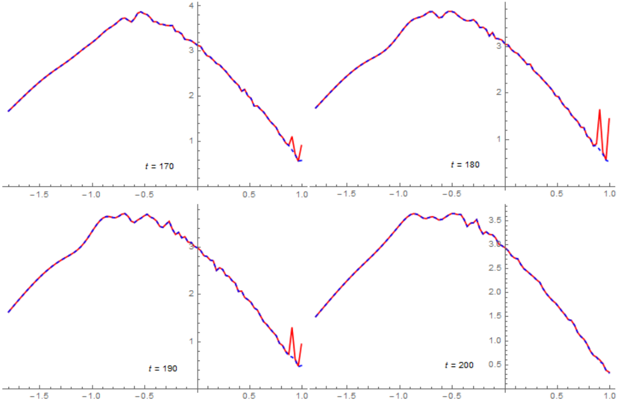

Figure: In contrast, the energy injected at the UV is dissipated away rapidly, having no effect on elsewhere of the kinetic energy spectrum.

Conclusion

- We have proposed an efficient method to obtain the QNM of holographic systems in the coupled case.
- By the fully nonlinear dynamic evolution of holographic systems, we have found that the dynamic stability of the BHMRS model is consistent with its thermodynamics stability.
- Quantum turbulence has been studied within the framework of a BEC-like holographic superfluid, with the following (possibly) universal features found:
  - Late time linearly decaying law for the inverse vortex number $N(t)^{-1}$
  - The Kolmogorov $-5/3$ scaling for the kinetic energy spectrum in the inertial range
  - The direct energy cascade in the inertial range

Discussion

- Snake instability of the superfluid soliton (with M. Guo, E. Keski-Vakkuri and H. Zhang, in finalizing)
- Striped configuration, optical lattice, ...
- The zero temperature (or low temperature) limit?
- Take into account back-reaction?

Remarks

- Holography offers a very important method for one to understand dynamics of strongly coupled quantum many-body systems, especially at finite temperature (with dissipation).
- There are still many theoretical problems as well as technical difficulties to overcome in holographic approaches.

Thanks for your attention!